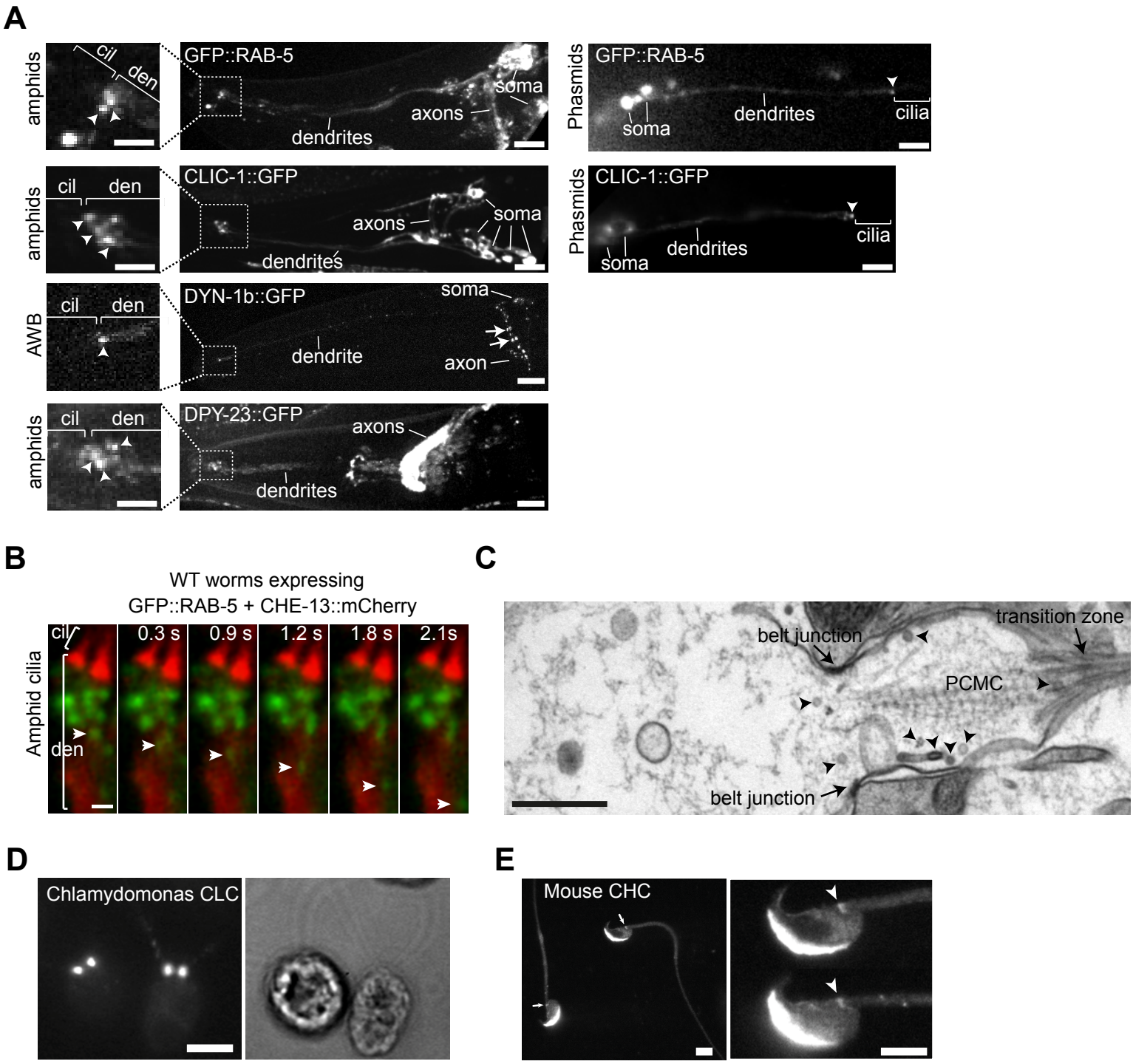

Figure S1, related to Figure 1. (A) Representative whole cell images of *C. elegans* ciliated sensory neurons showing the subcellular localisation of endocytic components. Shown are fluorescence images of head and tail regions of worms overexpressing the indicated GFP-tagged transgenes in amphid or phasmid neurons with the exception of *dyn-1*, which is expressed only in the AWB neurons. Arrowheads indicate an enriched pool of protein found at the distal tips of dendrites, beneath the presumptive cilia, in a region we call the periciliary membrane compartment (PCMC). Arrows indicate DYN-1b localisation at presumptive presynaptic sites. Transgenes expressed under gene promoters active in ciliated cells, namely *che-12* (CLIC-1, CHE-13) [1], *arl-13* (RAB-5) [2, 3], *rab-3* (DPY-23) [4, 5] and *str-1* (DYN-1b) [6]. Scale bars; 2 μm (high magnification images) and 5 μm (low magnification images). cil; cilia. den; dendrite. **(B)** Time lapse images showing the movement of a GFP::RAB-5 associated vesicle (arrowhead) from the ciliary base region (marked with CHE-13::mCherry) towards the cell soma. c; ciliary axonemes, D; dendrite. Scale bar; 1 μm. s; seconds. A representative movie is shown in movie 1. **(C)** Longitudinal transmission electron microscopy image of a WT ciliated cell showing the transition zone, PCMC (demarked by the ciliary transition zone at the distal end and a belt junction at the proximal end) and a more proximal dendrite compartment. Arrowheads denote vesicles, almost all of which are in the PCMC. A ciliary rootlet is seen to extend proximally from the transition zone. Scale bar; 500 nm. **(D)** Clathrin light chain (CLC) localises to the flagellar base in Chlamydomonas. Left is fluorescence image from immunostaining with CLC antibody; right is brightfield image. Scale bar; 5 μm. **(E)** Immunostaining shows a pool of clathrin heavy chain (CHC) at the flagellar base in mouse sperm (arrows; arrowheads). Magnified views of sperm in left image are shown in right image. Scale bars; 5 μm.

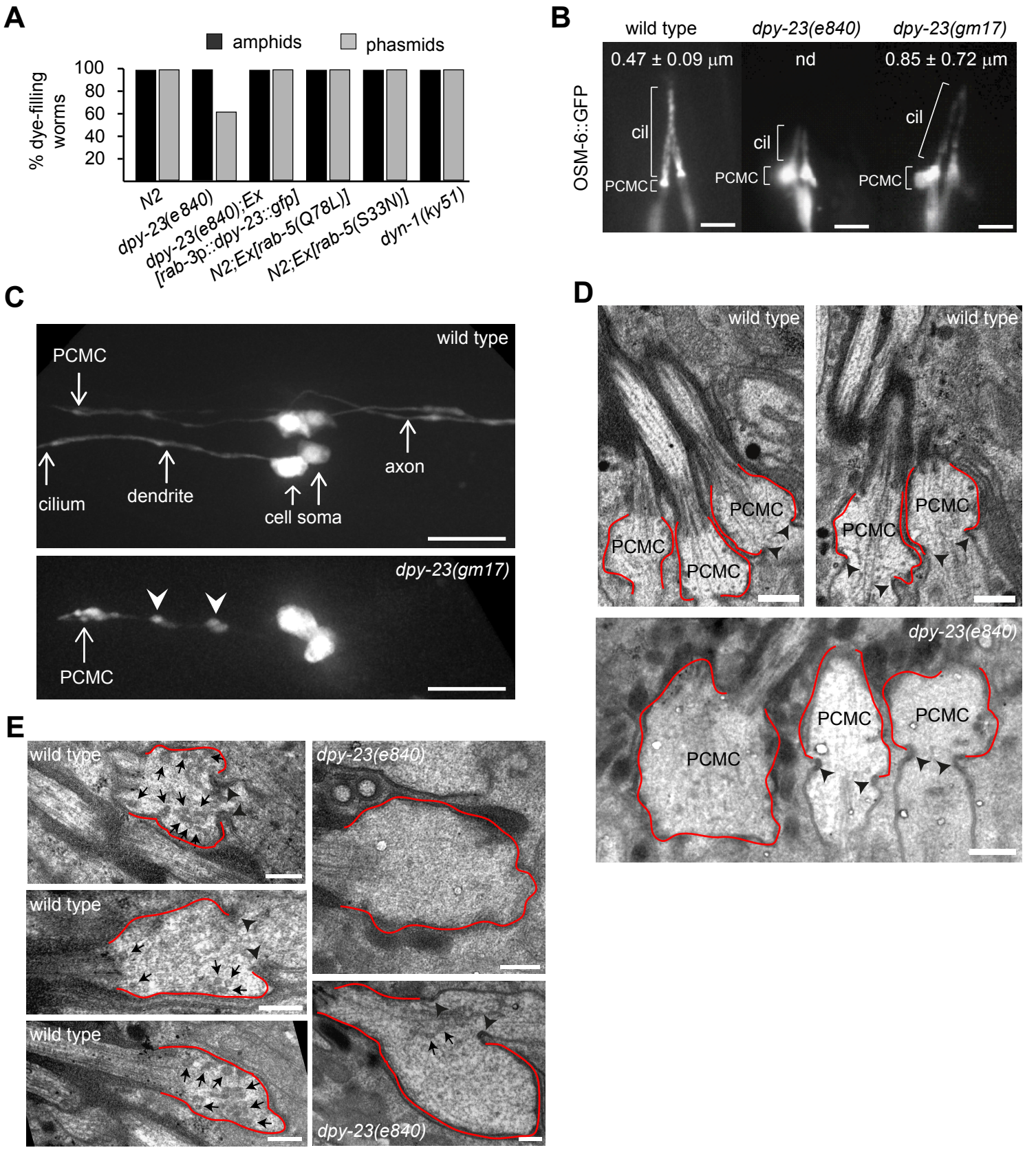

Figure S2, related to Figure 2. *C. elegans* endocytic gene mutants exhibit mostly normal dye-filling characteristics but display expanded ciliary and PCMC membranes. **(A)** Shown are percentage of worms of the indicated genotypes exhibiting normal uptake of fluorescent dye (DiI). >50 worms analysed for each strain. **(B)** Representative fluorescence images of PHA/B cilia from worms of the indicated genotypes expressing *osm-6/IFT52::gfp* which marks cilia (cil) and the region immediately beneath the transition zone at the distal end of the periciliary membrane compartment (PCMC) [7]. Average PCMC areas of PHA/B neurons are shown (n>25). nd; not determined. Scale bars; 3 μm. **(C)** Whole cell images of PHA/B neurons expressing the transcriptional marker *srb-6*p::*gfp*. Arrowheads; expanded membrane patches of dendrite regions other than the PCMC. Scale bars; 15 μm. **(D, E)** Images from longitudinal sections of amphid channel cilia showing enlarged PCMCs (demarked in red) in *dpy-23(e840)* mutants compared with WT controls. Arrowheads; belt junctions. Vesicles indicated by arrows. Images in E (scale bars; 250 nm) are a higher magnitude than D (scale bars; 500 nm). Images with apparent 'closed' PCMCs are due to sectioning above the plane of the belt junctions and more proximal dendrite regions.

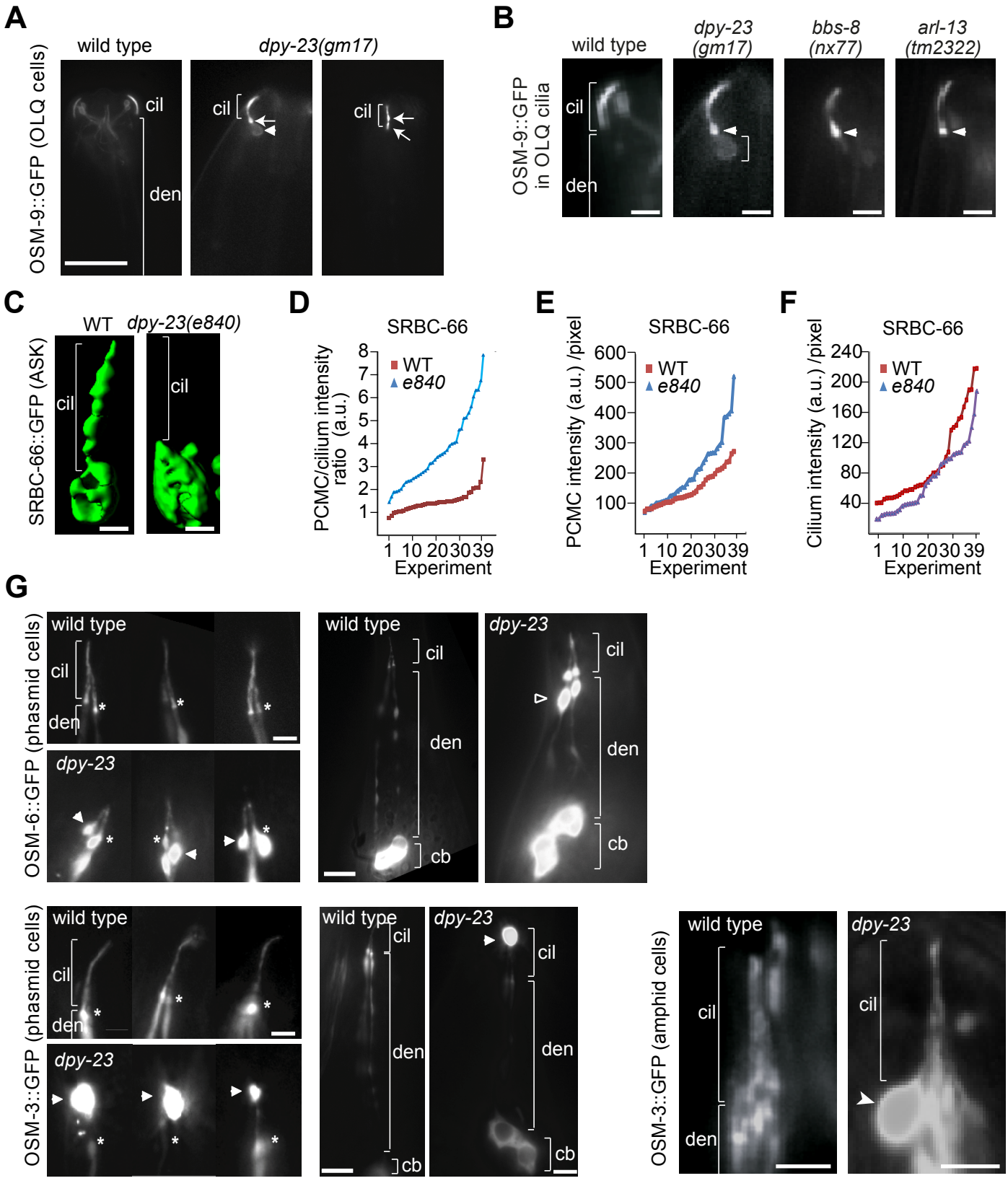

Figure S3, related to Figure 4. Representative cilium and whole cell images of ciliary protein localisations in AP-2-disrupted worms. **(A)** Whole cell fluorescence images of worms expressing *osm-9::gfp* (OLQ cells). Scale bar; 10 μm. Arrowhead denotes periciliary membrane compartment; arrows denote abnormal punctate straining. **(B)** Comparison of OSM-9::GFP localisation in the indicated genotypes. Arrowhead denotes abnormal punctate staining at the distal end of the PCMC. Scale bars; 2 μm. **(C)** Deconvoluted and volume rendered images showing SRBC-66::GFP at the periciliary membrane beneath the ASK cilium. Note that the absence of SRBC-66 ciliary staining in the *e840* mutants is an extreme example as ciliary staining (albeit reduced in some cases) is typically observed. Scale bars; 0.5 μm. **(D-F)** Profiles of 39 SRBC-66 signal intensity measurement experiments in the PCMC and cilium of WT and *dpy-23(e840)* ASK neurons. All data acquired from images taken at identical exposure settings and background subtracted. Data in E and F are also adjusted for area. a.u.; arbitrary units. **(G)** Fluorescence images of PHA/PHB cilia (left-hand images) and whole cells (right-hand images) in wild type and *dpy-23(e840)* worms overexpressing *osm-3/KIF17::gfp* or *osm-6/IFT52::gfp* transgenes. Accumulation of OSM-6::GFP in the presumptive expanded PCMC is indicated by filled arrowheads and in more proximal regions by clear arrowheads. OSM-3::GFP accumulation in ciliary tips is indicated by arrowheads. Asterisks denote ciliary base. cb; cell body, cil; cilia, den; dendrite. Scale bars; 3 μm (cilia images); 5 μm (whole cell images).

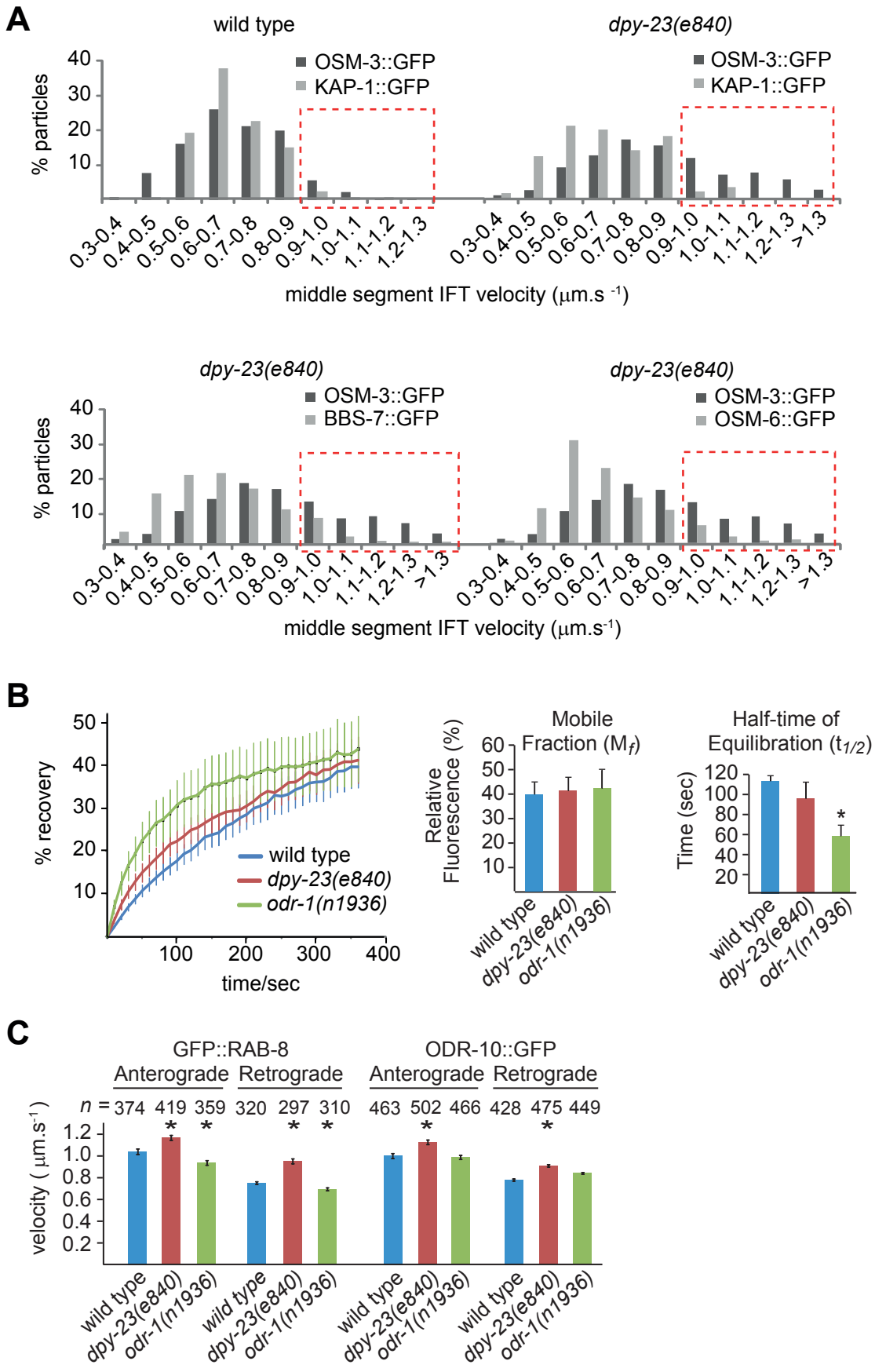

Figure S4 related to Table 1. Intraflagellar transport (IFT) and dendritic vesicular transport in AP-2 disrupted worms. **(A)** Rate profiles of anterograde IFT velocities (mostly amphid channel cilia) for OSM-3::GFP, KAP-1::GFP (kinesin-II subunit), OSM-6 (IFT-B protein; IFT52) and BBS-7 (BBSome subunit) in WT and *dpy-23(e840)* mutant worms. Dashed red box indicates fast moving sub-populations of OSM-3::GFP in middle segments. Number of particles analysed for each strain is shown in Table 1. **(B)** Kinetics of fluorescence recovery following photobleaching of ODR-10::GFP signals in the distal portion of AWB cilia in the indicated strains expressing the *srd-23*p*::odr-10::gfp* transgene. All analysed cilia fall into category 2, as defined in Figure 2C. **(C)** Transport velocities of ODR-10::GFP and GFP::RAB-8 vesicles along AWB dendrites in anterograde (towards cilium) and retrograde (towards cell soma) directions. All velocity measurements were computed from kymographs derived from time-lapse movies. For (B) and (C), >10 animals were analysed for each genotype. For (C), *n*; number of particles analysed. Error bars; SEM. * p<0.001, compared to WT (one-way ANOVA followed by Bonferroni's post-hoc test).

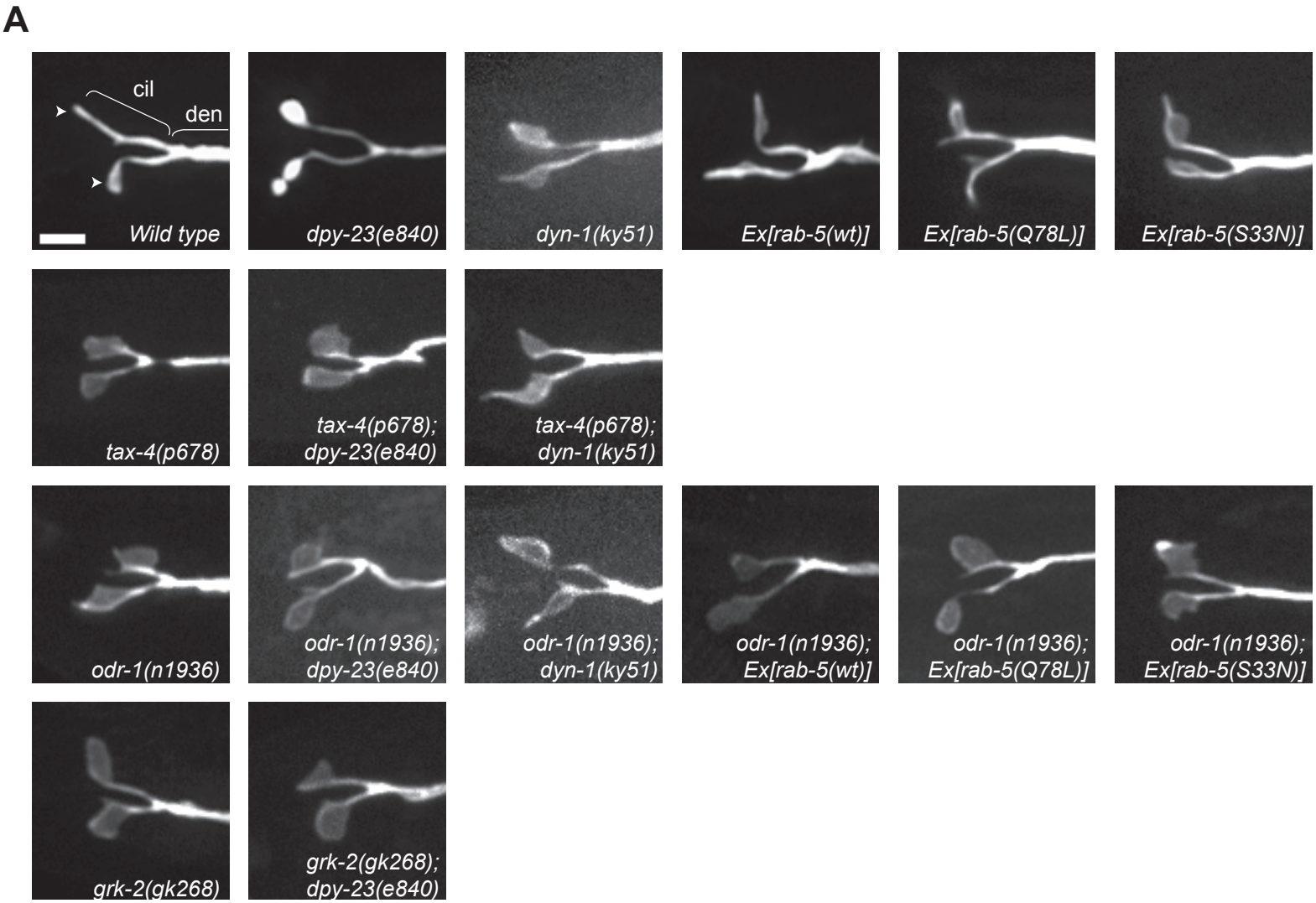

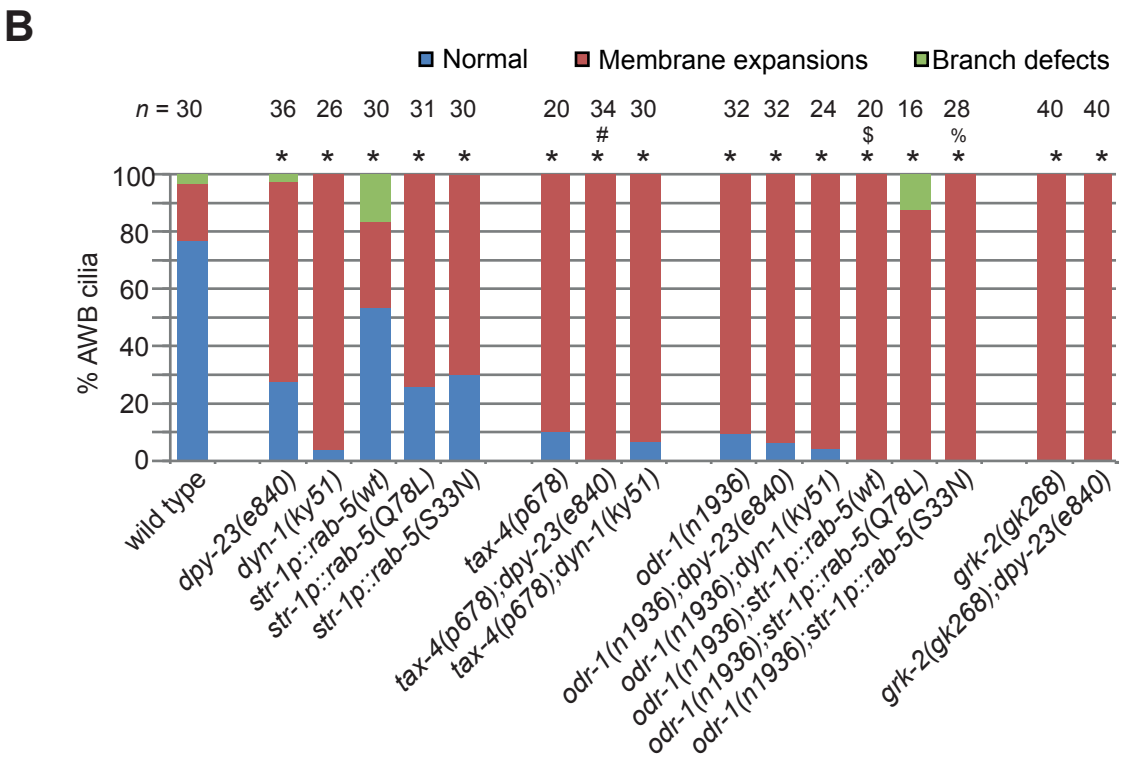

Figure S5, related to Figure 5. Representative images and analysis of AWB cilium morphologies in single and double mutants of sensory signaling and endocytosis genes. **(A)** Representative images all identically orientated and scaled. cil; cilium. den; dendrite. Scale bar; 3 μm. **(B)** Categorisation of AWB cilium phenotypes. n; number of cilia analysed. p<0.001 (cross-tabs and Chi-square test; compared with * WT, # *dpy-23(e840)*, $ *str-1p::rab-5(wt)* or % *str-1p::rab-5(S33N)*).

SUPPLEMENTAL MOVIE LEGEND

Movie 1. GFP::RAB-5 activity beneath amphid sensory cilia. Shown is a time-lapse movie from the amphid ciliary region of worms co-expressing *arl-13*p*::gfp::rab-5* and *che-12*p*::che-13::mcherry*. CHE-13::mCherry marks the ciliary axonemes. Note RAB-5-associated particles (vesicles) emerging from ciliary base region and moving towards the cell soma. Movie played at 5 frames per second (original time-lapse taken at 3 frames per second).

SUPPLEMENTAL EXPERIMENTAL PROCEDURES

C. elegans strains, alleles and transgenes

C. elegans worms were maintained and cultured at 20°C using standard techniques [8]. Strains/alleles: *C. elegans* variety Bristol strain N2, *dpy-23(e840), dpy-23(gm17), rab-8(tm2526), dyn-1(ky51), tax-4(p678), odr-1(n1936), grk-2(gk268), bbs-8(nx77), klp-11(tm324), osm-3(p802)* and *che-2(e1033)*. Transgenic strains containing transcriptional fusion genes were: *kyIs104[str-1*p*::gfp]*, *kyIs136[str-2*p*::gfp]*, *kyIs164[gcy-5*p*::gfp]*, *gmIs13[srb-6*p*::gfp]*, and *pkIs519[gpa-6*p*::gfp]*. Transgenic strains containing translational fusion transgenes were: *myEx10[che-11*p*::che-11::gfp]*, *myEx10[che-12*p*::che-13::mCherry]*, *mnIs17[osm-6*p*::osm-6::gfp]*, *ejEx[kap-1*p*::kap-1::gfp]*, *ejEx[osm-3*p*::osm-3::gfp]*, *oxEx730[dpy-23*p*::dpy-23::gfp]* (kind gift from Dr. Erik M. Jorgensen), *oxEx789[rab-3p::dpy-23::gfp]* (E. Jorgensen), *nsEx[che-12*p*::clic-1::gfp]* (kind gift from Dr. Shai Shaham), *nsEx[che-12*p*::che-13::mCherry]* (S. Shaham), *oqEx203[arl-13*p*::gfp::rab-5]*, *oqEx204[arl-13*p*::gfp::rab-5(Q78L)]*, *oqEx205[arl-13*p*::gfp::rab-5(S33N)]*, *oyEx501[str-1*p*::dyn-1b::gfp]*, *oqEx209[str-1*p*::odr-10::tdTomato]*, *kyIs53[str-*

*1*p*::odr-10::gfp]*, *oqEx58[arl-13*p*::arl-13::gfp]*, *oyEx502[srd-23*p*::odr-10::gfp]*, *oyEx503[srd-23*p*::gfp::rab-8]*, *oyEx504[str-1*p*::rab-5(wt)]*, *oyEx505[str-1*p*::rab-5(Q78L)]*, *oyEx506[str-1*p*::rab-5(S33N).* Strains containing *rab-5* knockdown constructs were: *oyEx507[sru-38p::rab-5(sense) + sru-38*p*::rab-5(antisense)]*. Coinjection markers used were *lin-15(+), unc-122*p*::dsRed* or pRF4. Introduction of transgenes into mutant backgrounds and double mutant strains were generated using standard genetic crosses. Homozygosity of the mutant alleles was confirmed via amplification from genomic DNA or via visible phenotypes.

Generation of *C. elegans* fluorescence protein-tagged constructs/transgenes

The following constructs were generated using a fusion PCR strategy [9]: *arl-13*p*::gfp::rab-5*, *arl-13*p*::gfp::rab-5(Q78L)*, *arl-13*p*::gfp::rab-5(S33N)* and *str-1*p*::odr-10::tdTomato*. *gfp*::*rab-5(WT)*, *gfp::rab-5(Q78L)* and *gfp::rab-5(S33N)* fragments were amplified from plasmids containing *vha-6*p*::gfp::rab-5* (generous gift of Barth Grant, Rutgers University, USA), *vha-6*p*::gfp::rab-5(Q78L)* (generous gift of Xiaochen Wang, National Institute of Biological Sciences, Beijing, China) and *vha-6*p*::gfp::rab-5(S33N)* (X. Wang). *str-1*p*::dyn-1b::gfp* plasmids constructs were designed via a Gateway cloning strategy. *dyn-1b* was amplified from cDNA. *str-1*p*::rab-5(wt/Q78L/S33N)*, *srd-23*p*::odr-10::gfp*, and *srd-23*p*::gfp::rab-8* plasmids were constructed by standard cloning techniques using *rab-5*, *odr-10*, and *rab-8* cDNAs, respectively. *che-12*p*::clic-1::gfp* plasmid was a kind gift of S. Shaham.

Generation of cell-specific RNAi constructs

Cell-specific RNAi constructs for the knock-down of *rab-5* in AWB and ASH were designed as described by Esposito *et al.* (2007) [10]. The *sru-38* promoter (1.9 kb) was fused

via PCR to sense or antisense *rab-5* genomic DNA (1.5 kb). Both *sru-38*p*::rab-5(sense)* and *sru-38p::rab-5(antisense)* constructs were injected at 100 ng/µl with *unc-122*p*::dsRed* (50 ng/µl) into *kyIs104[str-1*p*::gfp]* animals [11].

Transmission electron microscopy (TEM)

TEM of amphid channel cilia was performed as described [3].

***C. elegans* fluorescence microscopy and IFT/dendritic compartment motility assays**

Fluorescence microscopy, IFT transport and ODR-10 dendritic transport assays were conducted as described previously [3, 6, 12]. For ODR-10::GFP and GFP::RAB-8 dendritic transport assays, fluorescence micrographs of fluorescently-tagged proteins were captured with a QuantEM 512SC EMCCD camera (photometrics), operating on a Zeiss motorised inverted research microscope (Axio Observer.Z1) coupled to a spinning disk confocal head (Yokogawa CSU-X1) and 488 nm laser excitation. For time-lapse imaging, SlideBook software was used to stream-capture images at consistent exposures of 300 msec and gain/offset settings. Resulting stacked TIFF images were processed into kymographs using the multiple kymograph plug-in for ImageJ software (National Institutes of Health; J. Rietdorf & A. Seitz/EMBL). Kymographs were analysed with ImageJ and calculations were performed in Microsoft Excel.

Fluorescence recovery after photobleaching (FRAP) assay

For FRAP, photobleaching of ODR-10::GFP ciliary signals was performed using a MicroPoint laser system (Photonic Instruments) equipped with an NL100 nitrogen laser (Stanford Research Systems) and images were captured using the microscopy system described for dendritic transport. The same settings (equivalent laser intensity [40%],

repetition [10], and exposure time [100 ms], gain/offset, and photobleaching area) were applied to all FRAP experiments. Fluorescence recovery across an image stack volume was recorded every 10 seconds using SlideBook software. Images were processed and analysed with ImageJ software (National Institutes of Health); StackReg and TurboReg plug-ins (P. Thévenaz, Biomedical Imaging Group, Swiss Federal Institute of Technology Lausanne) were used to compensate for xy movements during acquisition. Data for mean fluorescence intensities of maximum-projected images were gathered from the bleached area (distal portion of cilium), a background area (a region outside cilium), and total ciliary intensity (to correct for the photobleached fraction as well as acquisition photobleaching). Selected regions from the bleached area and background were of the same size and area. Intensity values (arbitrary units) for these selected regions were calculated using ImageJ. For each image, at each timepoint, absolute intensity values were calculated for the photobleached and total ciliary intensity regions by subtracting the background area value. Intensity ratios of the photobleached to total ciliary area values were then derived, and subsequently normalized against pre-bleach ratio values (i.e. to set the pre-bleach values to 100%). Percentage recovery of signal following photobleach was then plotted against time post-photobleach. Qualitative information from FRAP experiments including mobile (M_f) and immobile (I_f) fractions as well as the half-time of equilibration ($t_{1/2}$) were calculated as described [13].

Chlamydomonas and mouse sperm clathrin localisation

Chlamydomonas CC-125 wild type mt+ 137c were a gift of Professor Gianni Piperno, Mount Sinai School of Medicine, New York, NY, USA, and were grown in “Medium R” (Sager and Granick rich medium) with or without calcium. Mouse semen samples were obtained from Jackson Labs (Bar Harbor, ME, USA). 200µl of autolysin treated *Chlamydomonas*, or mouse serum samples, was pipetted onto lysine coated coverslips and

fixed in 2ml of 4% PFA. Primary antibodies included Covance mono-clonal mouse-anti-clathrin light chain (con.1) and Abcam poly-clonal goat-anti-clathrin heavy chain. Cells were imaged with an Olympus IX81 inverted fluorescence microscope at 60x (*Chlamydomonas*) or 100x (sperm) magnification.

SUPPLEMENTAL REFERENCES

1. Bacaj, T., Lu, Y., and Shaham, S. (2008). The conserved proteins CHE-12 and DYF-11 are required for sensory cilium function in Caenorhabditis elegans. Genetics *178*, 989-1002.
2. Blacque, O.E., Perens, E.A., Boroevich, K.A., Inglis, P.N., Li, C., Warner, A., Khattra, J., Holt, R.A., Ou, G., Mah, A.K., et al. (2005). Functional genomics of the cilium, a sensory organelle. Curr Biol *15*, 935-941.
3. Cevik, S., Hori, Y., Kaplan, O.I., Kida, K., Toivenon, T., Foley-Fisher, C., Cottell, D., Katada, T., Kontani, K., and Blacque, O.E. (2010). Joubert syndrome Arl13b functions at ciliary membranes and stabilizes protein transport in Caenorhabditis elegans. The Journal of cell biology *188*, 953-969.
4. Gu, M., Schuske, K., Watanabe, S., Liu, Q., Baum, P., Garriga, G., and Jorgensen, E.M. (2008). Mu2 adaptin facilitates but is not essential for synaptic vesicle recycling in Caenorhabditis elegans. The Journal of cell biology *183*, 881-892.
5. Nonet, M.L., Staunton, J.E., Kilgard, M.P., Fergestad, T., Hartwieg, E., Horvitz, H.R., Jorgensen, E.M., and Meyer, B.J. (1997). Caenorhabditis elegans rab-3 mutant synapses exhibit impaired function and are partially depleted of vesicles. J Neurosci *17*, 8061-8073.
6. Mukhopadhyay, S., Lu, Y., Shaham, S., and Sengupta, P. (2008). Sensory signaling-dependent remodeling of olfactory cilia architecture in C. elegans. Developmental cell *14*, 762-774.
7. Williams, C.L., Li, C., Kida, K., Inglis, P.N., Mohan, S., Semenec, L., Bialas, N.J., Stupay, R.M., Chen, N., Blacque, O.E., et al. (2011). MKS and NPHP modules cooperate to establish basal body/transition zone membrane associations and ciliary gate function during ciliogenesis. The Journal of cell biology *192*, 1023-1041.
8. Brenner, S. (1974). The genetics of Caenorhabditis elegans. Genetics *77*, 71-94.
9. Hobert, O. (2002). PCR fusion-based approach to create reporter gene constructs for expression analysis in transgenic C. elegans. BioTechniques *32*, 728-730.
10. Esposito, G., Di Schiavi, E., Bergamasco, C., and Bazzicalupo, P. (2007). Efficient and cell specific knock-down of gene function in targeted C. elegans neurons. Gene *395*, 170-176.
11. Troemel, E.R., Kimmel, B.E., and Bargmann, C.I. (1997). Reprogramming chemotaxis responses: sensory neurons define olfactory preferences in C. elegans. Cell *91*, 161-169.
12. Kaplan, O.I., Molla-Herman, A., Cevik, S., Ghossoub, R., Kida, K., Kimura, Y., Jenkins, P., Martens, J.R., Setou, M., Benmerah, A., et al. (2010). The AP-1 clathrin

adaptor facilitates cilium formation and functions with RAB-8 in C. elegans ciliary membrane transport. Journal of cell science *123*, 3966-3977.

13. Bancaud, A., Huet, S., Rabut, G., and Ellenberg, J. (2010). Fluorescence perturbation techniques to study mobility and molecular dynamics of proteins in live cells: FRAP, photoactivation, photoconversion, and FLIP. Cold Spring Harb Protoc *2010*, pdb top90.